1-4-2019

Cortactin Phosphorylation by Casein Kinase 2 Regulates Actin-Related Protein 2/3 Complex Activity, Invadopodia Function and Tumor Cell Invasion

Steven M. Markwell
West Virginia University

Amanda G. Ammer
West Virginia University

Erik T. Interval
West Virginia University

Jessica L. Allen
West Virginia University

Brenen W. Papenberg
West Virginia University

See next page for additional authors

HHS Public Access

Author manuscript

Mol Cancer Res. Author manuscript; available in PMC 2020 April 01.

Published in final edited form as:

Mol Cancer Res. 2019 April ; 17(4): 987–1001. doi:10.1158/1541-7786.MCR-18-0391.

Cortactin Phosphorylation by Casein Kinase 2 Regulates Actin-Related Protein 2/3 Complex Activity, Invadopodia Function and Tumor Cell Invasion

Steven M. Markwell[1], **Amanda G. Ammer**[1], **Erik T. Interval**[2], **Jessica L. Allen**[1], **Brenen W. Papenberg**[1], **River A. Hames**[1], **Johnathan E. Castaño**[2], **Dorothy A. Schafer**[3], and **Scott A. Weed**[1,*]

[1]Program in Cancer Cell Biology, Department of Biochemistry, West Virginia University, Morgantown, WV

[2]Department of Otolaryngology, Head and Neck Surgery, West Virginia University, Morgantown, WV

[3]Department of Biology, University of Virginia, Charlottesville, VA.

Abstract

Malregulation of the actin cytoskeleton enhances tumor cell motility and invasion. The actin-binding protein cortactin facilitates branched actin network formation through activation of the actin-related protein (Arp) 2/3 complex. Increased cortactin expression due to gene amplification is observed in head and neck squamous cell carcinoma (HNSCC) and other cancers, corresponding with elevated tumor progression and poor patient outcome. Arp2/3 complex activation is responsible for driving increased migration and extracellular matrix (ECM) degradation by governing invadopodia formation and activity. While cortactin-mediated activation of Arp2/3 complex and invadopodia regulation has been well established, signaling pathways responsible for governing cortactin binding to Arp2/3 are unknown and potentially present a new avenue for anti-invasive therapeutic targeting. Here we identify casein kinase (CK) 2α phosphorylation of cortactin as a negative regulator of Arp2/3 binding. CK2α directly phosphorylates cortactin at a conserved threonine (T24) adjacent to the canonical Arp2/3 binding motif. Phosphorylation of cortactin T24 by CK2α impairs the ability of cortactin to bind Arp2/3 and activate actin nucleation. Decreased invadopodia activity is observed in HNSCC cells with expression of CK2α phosphorylation-null cortactin mutants, shRNA-mediated CK2α knockdown, and with the CK2α inhibitor Silmitasertib. Silmitasertib inhibits HNSCC collective invasion in tumor spheroids and orthotopic tongue tumors in mice. Collectively these data suggest that CK2α-mediated cortactin phosphorylation at T24 is critical in regulating cortactin binding to Arp2/3 complex and pro-invasive activity, identifying a potential targetable mechanism for impairing HNSCC invasion.

[*]**Corresponding Author:** Scott A. Weed, West Virginia University Cancer Institute, P.O. Box 9300, Morgantown, WV 26506, Phone: 304-293-3016, Fax: 304-293-4667, scweed@hsc.wvu.edu.

Disclosure of Potential Conflicts of Interest: This laboratory was supported in part by a grant from Gilead Sciences during the period when the work was conducted. Gilead grant funds were not used to support any aspect of the project reported in this manuscript. Gilead Sciences had no input on the findings disclosed herein.

Implications: This study identifies a new signaling pathway that contributes to enhancing cancer cell invasion.

Graphical abstract

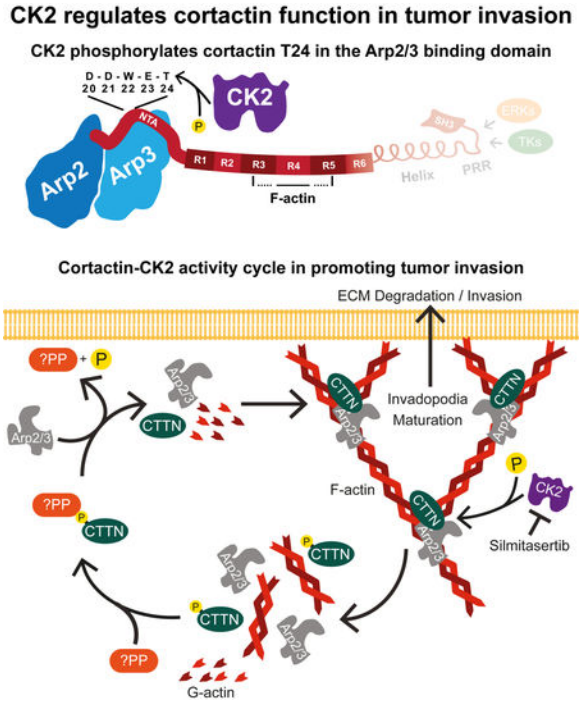

Keywords

Cortactin; HNSCC; Invadopodia; Arp2/3; CK2

Introduction

Cell invasion from the primary tumor is responsible for initiating the metastatic cascade and increasing cancer lethality (1,2). Invasion is initiated in part through the action of invadopodia, actin-based membrane protrusions produced by tumor cells that mediate dissemination by degrading restrictive extracellular matrix (ECM) proteins through enzymatic matrix metalloproteinase (MMP) activity (3). Invadopodia contain a central filamentous (F-) actin core surrounded by an integrin-based adhesion ring complex that anchors the structure to allow focal matrix degradation and tumor cell protrusion through the basement membrane (4). Cortactin and actin-related protein (Arp) 2/3 complex are essential protein components involved in invadopodia precursor core formation required for subsequent MMP recruitment and membrane protrusion (5,6). Cortactin overexpression is common in several cancer types including head and neck squamous cell carcinoma (HNSCC), resulting in enhanced motility, invasion, and invadopodia activity (7,8). Cortactin binding to Arp2/3 complex activates Arp2/3 actin nucleation activity, enhancing cellular actin polymerization to form branched F-actin networks (6,8–10). Cortactin also directly binds F-actin and bundles newly-formed filaments, providing an overall stabilizing effect on the Arp2/3-F-actin network required for invadopodia formation (5,6,11). Previous work has

shown that a DDW motif within the cortactin N-terminal acidic (NTA) domain is central in mediating Arp2/3 activation and branched actin network formation (7,12–14). This region is similar to the Arp2/3 binding motif found in the Acidic region of the Verprolin, Central, Acidic (VCA) domain of the Wiskott-Aldrich Syndrome protein (WASp)-family of Arp2/3 nucleation promotion factors (NPFs). While the cortactin DDW motif is well established as the region responsible for Arp2/3 binding, post-translational or other modifications of amino acids in the NTA region that regulate binding have not been reported. Tyrosine and serine phosphorylation of cortactin residues in the carboxyl-terminal region are essential for invadopodia formation, cellular invasion, and tumor metastasis through multiple mechanisms ultimately involving activation of WASp NPFs (6,7,15–18). In addition, comprehensive phosphorylation site mapping by mass spectroscopy has identified NTA phosphorylation sites in close proximity to the DDW motif (19). This raises the possibility that phosphorylation of one or more of these residues may serve to govern Arp2/3 binding and invadopodia function in invasive cancer.

Casein kinase (CK) 2 is a ubiquitously expressed, constitutively active serine/threonine kinase consisting of two catalytic subunits (α or α') and two β regulatory subunits (20). Increased CK2 expression correlates with cell cycle progression, apoptosis resistance and tumor cell motility in various cancers (20). Overexpressed CK2 enhances HNSCC tumor cell motility (20). CK2 phosphorylates the cortactin homologue HS1 at an unidentified site(s) in the NTA region (21), as well as residues near the DDW region in the NPFs neuronal (N)-WASp and WAS protein family member 2 (WASF2; WAVE2, WASp family Verprolin-homologous protein 2) (22–25). Here we show that CK2 phosphorylation of threonine (T) 24 in the cortactin NTA impairs binding to and activation of Arp2/3 complex. Cortactin T24 and CK2 are required for efficient invadopodia formation and ECM degradation activity in HNSCC cell lines. Treatment of established and primary HNSCC cells with the selective CK2 inhibitor Silmitasertib impairs invadopodia function and regional HNSCC invasion. These results identify a new mechanism of invadopodia regulation that can be targeted to impair HNSCC invasion.

Materials and Methods

Cell culture, lentiviral infection and transfection, siRNA

HNSCC cell lines OSC19 and UMSCC1 were acquired and maintained as described (26). MDA1586 cells were obtained in March 2014 from Barbara Frederick (University of Colorado, Denver, CO). All HNSCC lines were authenticated by STR profiling at the University of Arizona Genetics Core in June 2017. PCR-based mycoplasma testing (13100-01, Southern Biotech) was conducted on OSC19 and UMSCC1 lines in March 2015 and were free of contamination. The MDA1586 line was not tested for mycoplasma. HEK293T/17 cells were obtained in April 2013 from Robert Wysolmerski (West Virginia University, Morgantown, WV). NIH3T3 cells were obtained in June 2017 from Ivan Martinez (West Virginia University, Morgantown, WV) and maintained for ≤10 passages. These lines were not authenticated or tested for mycoplasma. Cells were propagated in DMEM supplemented with 10% fetal bovine serum and 1% penicillin-streptomycin for < 6 months. OSC19 and UMSCC1 cells stably infected with pLKO.1-puro cortactin shRNA or

CK2α shRNA were generated by clonal puromycin selection following standard methods (CSNK2A1: TRCN0000380839, TRCN0000027627; CTTN: TRCN0000040275).

UMSCC1 cells stably infected with pLU-Luc2 expressing luciferase were generated following standard methods. Murine cortactin rescue OSC19 and UMSCC1 cells containing cortactin shRNA stably infected with pLenti CMV Hygro cortactin constructs were generated by subsequent clonal hygromycin selection. Complete cortactin knockdown in OSC19 and UMSCC1 cells was achieved by transfection of cortactin-targeting siRNA (ON-TARGETplus SMARTpool L-010508-00-0020, Dharmacon) using a Nucleofector I (Amaxa Biosystems).

Western blotting, antibodies and immunoprecipitation

Western blotting was conducted as described (27) and visualized with autoradiography film (E3012, Denville Scientific) or captured by an Amersham Imager 600 (GE Healthcare Bio-Sciences). Antibodies used were: anti-cortactin clone 4F11 (1 μg/ml, (26)), anti-pS473 AKT (#4060, 1:1000; Cell Signaling Technology), anti-panAKT (#2920, 1:1000; Cell Signaling Technology), anti-β-actin (#8457, 1:1000; Cell Signaling Technology), anti-CK2α (#2656, 1:500, Cell Signaling Technology), anti-DYKDDDK (FLAG) clone 2EL-1B11 (MAB3118, 1:500, Millipore) and anti-Arp3 (#07-272, 1:500, EMD Millipore). Immunoprecipitation was conducted from cells lysed in 50 mM Tris Buffer pH 8.0 with 10 mM EDTA and 1% NP-40 (28). Clarified lysates (1 mg) were incubated with 50 μl of FLAG M2 affinity resin (A2220, Sigma-Aldrich) for 2 hours at 4°C. Immune complexes were collected by centrifugation, washed twice with Tris buffer, separated by SDS-PAGE, and Western blotted with antibodies as described above.

Gelatin degradation assay, invadopodia characterization and microscopy

Cells were plated on Oregon Green 488-conjugated gelatin (G13186, Invitrogen) coated coverslips (29). In cases of inhibitor treatment, cells were allowed to attach for 1 hour, then incubated for 12 or 24 hours with Silmitasertib (S2248, Selleckchem) as indicated. Cells were rinsed in PBS, fixed with 10% buffered formalin (SF100-4, Fisher) and labeled as described (29). Antibodies used were 4F11 (1:500) or anti-FLAG (1:500). Primary antibodies were visualized using Alexa Fluor 647 conjugated goat anti-mouse secondary antibody (A21235, 1:500, Invitrogen). F-actin was visualized with rhodamine-conjugated phalloidin (R415, 1:1000, Invitrogen). Coverslips were mounted using ProLong Gold antifade with DAPI (P36935, Invitrogen). Images for quantifying gelatin degradation and knockdown/rescue expression were acquired with a Zeiss Axio Imager Z2 epifluorescent microscope equipped with an AxioCam MRm CCD camera and AxioVision software using LD Plan-Neofluar 40X/0.6 Corr and Plan-Apochromat 63X/1.4 oil objectives (Carl Zeiss Microscopy). Acquisition parameters were held constant within comparison groups. Confocal images were acquired using a Zeiss Axio Imager Z1 LSM510 confocal microscope with EC Plan-Neofluar 40X/1.30 and Plan-Apochromat 63X/1.4 oil objectives and Zen2009 software (Carl Zeiss Microcopy). All representative images were level adjusted to enhance contrast and brightness as needed and resized using Photoshop CC 2018 (Adobe Systems). Gelatin images were corrected for uneven illumination via bandpass filtering using ImageJ software (NIH). Degradation and invadopodia formation was quantified as described

previously (29), with n ≥ 70 lentiviral infected or ≥ 100 inhibitor-treated cells evaluated for each condition. FLAG-stained control images were thresholded against non-specific staining using ImageJ software. Cells above threshold values were considered positive for rescue construct expression and used for quantitation. For therapeutic treatments and RNAi stable cell lines, degradation and cell areas were determined by Image J (NIH) on an individual cell basis. Data represent the mean values normalized to control degradation area per cell area from at least 3 independent experiments. Invadopodia precursors were determined by colocalization of actin and cortactin at sites lacking gelatin degradation. Active invadopodia were determined by colocalization of actin, cortactin, and gelatin degradation. Data represent the mean from at least 3 independent experiments. Phase contrast images were acquired using a Zeiss Axiovert 200M microscope equipped with an AxioCamMR CCD camera using a Plan-Neofluar 10X/0.30 objective and AxioVision software (Carl Zeiss Microscopy).

CK2α kinase assay

In vitro kinase assays were performed as described (30). Briefly, 0.25, 0.5, or 1 μg of purified GST-WT or T24A cortactin NTA fusion proteins were incubated with 8 ng CK2α (#14-445, Millipore) and 10 μCi ^{32}Pγ-ATP (#NEG002A500UC, PerkinElmer) at 30°C for 10 minutes. Reactions were terminated with hot SDS sample loading buffer. Proteins were visualized by autoradiography. Purified N-WASp GST-VCA (0.5 μg) and GST (1 μg) were used as respective positive and negative controls.

In vitro cortactin phosphorylation binding assay

Purified WT or T24A cortactin proteins (2.5 μg) were bound to 4F11-conjugated protein G magnetic beads (#10003D, Life Technologies). Immune complexes were incubated in the presence or absence of activated CK2α (75 ng; #V4482, Promega) and ATP (500 nmoles, #BP413-25, Fisher Scientific) at 30°C for 15 minutes. Reactions were washed twice with 10 mM Tris pH 7.4, 150 mM NaCl, 0.5 mM EDTA. Complexes were washed once with 10 mM Tris pH 7.4, 10 mM EDTA and incubated with 50 ng Arp2/3 complex (#RP01-A, Cytoskeleton) at 4°C for 30 minutes. Following incubation, binding complexes were washed once with 10 mM Tris Buffer pH 7.4 with 25 mM NaCl, 10 mM EDTA, 1% NP-40, then boiled and Western blotted with antibodies against cortactin and Arp3.

Actin polymerization assay

Actin polymerization experiments were conducted as described previously (31). Reactions contained 2 μM actin (10% pyrene-labeled), 75 nM Arp2/3 complex, 100 nM cortactin or 50 nM GST-VCA (#VCG03, Cytoskeleton), and/or varying amounts of CK2α (#14-445, Millipore) as indicated. For reactions with CK2α, GST-VCA or cortactin mutants were preincubated with CK2α and 500 nmoles ATP for 15 minutes at room temperature prior to addition to the actin polymerization reaction.

PDX-derived cell lines

Patient-derived xenograft (PDX) tumors and cell lines were established as described (32). WVUSCC-AR2 and WVUSCC-AR5 were derived from surgical specimens of alveolar ridge

HNSCC in compliance with West Virginia University Institutional Review Board approved protocol #1310105737A033. PDXs were developed in compliance with West Virginia University Institutional Animal Care and Use Committee approved protocol #15-0302.6 by placing approximately 1 mm tumor fragments into subcutaneous pockets in the flanks of anesthetized 8-10 week old NOD/SCID-γ (NSG) mice. Tumor fragments were overlayed with Matrigel (354234, Corning) and incisions were closed using wound clips. Mice were weighed and monitored for tumor growth on a weekly basis. PDX tumors were passed into new NSG mice and/or used to generate cell lines once tumors reached ~1 cm in greatest dimension.

For cell line derivation, PDX tumors were minced and digested in DMEM supplemented with 20% FBS and 1 mg/mL collagenase IV (17104019, Gibco). Digested tissues were plated onto NIH3T3 fibroblasts senesced with 4 μg/mL mitomycin C (BP2531, Fisher) and cultured in DMEM:F12 1:1 supplemented with 10% FBS, 400 ng/mL hydrocortisone (H0888, Sigma), 50 μg/mL gentamycin (15750060, Gibco), 5 μM ROCK inhibitor (S1049, Selleckchem), 0.5 ng/mL recombinant human epidermal growth factor (EGF) (PHG0311, Gibco), and 10 ng/mL cholera toxin (C8062, Sigma). Both WVUSCC-AR2 and -AR5 were derived in August 2017 and maintained for ≤ 10 passages. Derived lines were verified using cytokeratin 14 staining (ab15462, Abcam). Neither STR profiling nor mycoplasma detection was performed on these cell lines. Prior to utilization in gelatin degradation or spheroid invasion assays, PDX derived cell lines were plated directly onto cell culture dishes for 1-2 passages to remove the fibroblast population. Gelatin degradation and spheroid invasion assays were performed in DMEM supplemented with 10% FBS.

In vitro tumor spheroid invasion

3D spheroid invasion assays were performed as previously described (26). 1×10^4 (OSC19) or 2.5×10^4 (UMSCC1 and WVUSCC-AR5) cells were plated into individual wells coated with 1.5% noble agar for 24 h (UMSCC1) or 48 h (OSC19 and WVUSCC-AR5) to form spheroids. For each line, spheroids were collected, resuspended in 500 μL of 2 mg/mL rat tail collagen I (354236, Corning), and plated into individual wells of a 24-well plate pre-coated with 400 μL solidified 2 mg/mL collagen I. Plates were incubated for 1 h at 37°C, then overlayed with 1 mL DMEM supplemented with 10% fetal bovine serum and 1% penicillin-streptomycin containing DMSO or 10 μM Silmitasertib. Spheroid invasion was visualized at the indicated time points by phase contrast microscopy using a Zeiss Axiovert 200M microscope equipped with an AxioCamMR CCD camera using a Plan-Neofluar 5X/0.15 objective and Axiovision software (Carl Zeiss Microscopy). Maximal radial distances for invaded cells were calculated using Axiovision software, with invasive distance determined as the difference between the initial and final maximum radius for each invaded spheroid.

Orthotopic tongue tumors and invasion analysis

Tongue tumor establishment was adapted from previous work (33). $2.5X10^4$ luciferase expressing UMSCC1 cells were injected into the tongues of 8-10 week old NSG mice (purchased from the West Virginia University Transgenic Animal Core Facility). Mice were maintained using transgenic dough diet (S3472, Bioserve) and weighed every 2-3 days.

Tumor growth was monitored by bioluminescent imaging using 150 mg/kg D-luciferin (122796, Caliper Life Sciences) injected intraperitoneally, followed by *in vivo* whole-body bioluminescence imaging using an IVIS Lumina-II system and Living Image 4.0 software (PerkinElmer). Tumors were allowed to establish for one week, then mice were divided equally into two groups based on approximate tumor size. Mice were given 50 mg/kg Silmitasertib in DMSO or DMSO alone by oval gavage twice daily for three weeks. Mice were subsequently euthanized, tongues excised, processed and stained for histological analysis.

To quantify invasion parameters, whole tongue histological images were cropped to encompass the tumor invasive front and analyzed using ImageJ. Images were processed with the colour deconvolution 1.5 plugin using H&E or H&E2 presets. Resultant colour_1 images were 25% contrast enhanced before conversion into binary images. ROIs were selected for particles above 15,000 pixel units and manually verified by overlay onto the original H&E image to remove artifacts. Invasive protrusions were defined as projections at the leading edge of the tumor surrounded by stroma on three sides and identified on the binary image using the polygon selection tool. Invasive distance was determined as the difference between the farthest edge of the protrusion and the protrusion base.

Statistical analysis

Differences in mean values between groups were evaluated using Student's or Welch's *t* test. Significance was determined at $p < 0.05$ utilizing GraphPad Prism 7 software. Error bars represent +/− S.E.M.

Results

Cortactin threonine 24 is required for Arp2/3 complex binding and activation

Phosphorylation of serine (S) 11, T13, and T24 in the murine cortactin NTA domain has been reported (19). The proximity of these residues to the canonical Arp2/3 binding motif consisting of amino acids 20-22 (DDW) has the potential to regulate Arp2/3 binding (Fig. 1A). To determine if these residues influence cortactin binding to Arp2/3, FLAG-tagged murine cortactin constructs were generated that contained serine to alanine (S11A) and threonine to alanine (T24A) phosphorylation-null mutations. T13 was not evaluated since it is not conserved in human cortactin. Co-immunoprecipitation studies indicate that S11A cortactin bound endogenous Arp2/3 at levels similar to wild-type (WT) cortactin, while T24A cortactin failed to effectively bind Arp2/3 despite retaining the DDW binding motif (Fig. 1B). Threonine to aspartic acid (T24D) phosphomimetic cortactin bound Arp2/3 at reduced levels compared to WT (Fig. 1B). These data demonstrate that both the DDW motif and T24 are required for optimal Arp2/3 complex binding. Furthermore, reduced Arp2/3 binding resultant from the addition of negative charge at amino acid 24 (T24D) suggests that phosphorylation may play a negative-regulatory role.

To assess the impact of T24 on Arp2/3 actin nucleation, recombinant human WT, ΔDDW, and T24A cortactin proteins were expressed in bacteria and purified (Fig. 1C). When evaluated in pyrene-labeled actin assembly assays, WT cortactin displayed slower

polymerization kinetics compared to the N-WASp VCA domain, whereas the ΔDDW mutant failed to activate Arp2/3 as previously reported (Fig. 1D, (16,34,35)). T24A cortactin demonstrated intermediate activity, with reduced nucleation levels compared to WT cortactin and increased nucleation compared to ΔDDW (Fig. 1D). Taken together these data identify T24 in the cortactin NTA as a critical residue required for optimal cortactin-mediated Arp2/3 binding and activation regardless of phosphorylation status.

Cortactin T24 is required for invadopodia-mediated ECM degradation

Cortactin is essential for initiating invadopodia formation, maturation, and ECM degradation in part due to NTA-mediated Arp2/3 binding (36,37). To determine the role of cortactin T24 in invadopodia function, a panel of cortactin knockdown-rescue cell lines stably expressing FLAG-cortactin mutant constructs were produced in invasive UMSCC1 (Fig. 2) and OSC19 (Supplementary Fig. S1) HNSCC cell lines. Both lines spontaneously produce invadopodia and degrade ECM (26,38). While individual cortactin siRNA (siCTTN) and shRNA (shCTTN) treatment resulted in decreased cortactin expression and matrix degradation in each case (Fig. 2D, Supplementary Fig. S1B, Supplementary Fig. S2), sequential exposure to cortactin siRNA in stable shRNA cells resulted in efficient and reliable cortactin knockdown (KD; Fig. 2, Supplementary Fig. S1, Supplementary Fig. S2). Cortactin KD cells were used for subsequent experimentation to minimize the possibility of residual endogenous cortactin masking the effects of re-expressed FLAG-cortactin mutants. FLAG-WT cortactin expression in KD cells partially restored the amount of active invadopodia formation in UMSCC1 cells (Fig. 2A & C) and fully restored ECM degradation in UMSCC1 (Fig. 2A & B) and OSC19 (Supplementary Fig. S1A & C) cell lines. FLAG-ΔDDW enhanced invadopodia precursor formation but failed to rescue active invadopodia and ECM degradation (Fig. 2A-C, Supplementary Fig. 1A & C). Similarly, both FLAG-T24A and FLAG-T24D cortactin restored invadopodia precursor formation while failing to induce invadopodia maturation above KD levels, with active invadopodia and ECM degradation levels for both mutants similar to that of FLAG-ΔDDW cortactin (Fig. 2A-C, Supplementary Fig. S1A, C, D). These results suggest that Arp2/3 binding and activation facilitated by cortactin T24 is required for effective cortactin-mediated invadopodia formation and ECM degradation in HNSCC cells.

CK2 phosphorylation of cortactin T24 regulates interaction with Arp2/3 complex

The importance of T24 in Arp2/3 activation and invadopodia function, along with prior identification of T24 as a cortactin phosphorylation site, led us to identify the kinase(s) responsible for phosphorylating T24. Computational analysis of the sequences flanking T24 was performed by seven independent predictive algorithms, six of which suggested that CK2α had the highest probability of phosphorylating cortactin T24 (Supplementary Table S1). To test this, kinase assays were conducted using GST-tagged cortactin WT and T24A NTA fusion proteins with purified active CK2α. The N-WASp VCA domain was used as a positive control, since previous studies have shown this region to be a CK2α substrate (23,25). Increasing amounts of GST-WT-NTA were efficiently phosphorylated by CK2α, whereas no phosphorylation was evident in GST-T24A-NTA (Fig. 3A). These data indicate that cortactin T24 can serve as a CK2α substrate, and that T24 is the only residue targeted by CK2α in the NTA region.

To determine if CK2α phosphorylation of cortactin T24 effects binding to Arp2/3 complex, recombinant human WT or T24A cortactin proteins were pre-incubated with or without CK2α, then mixed with purified Arp2/3. Phosphorylation of WT cortactin by CK2α reduced binding of Arp2/3 complex to background levels (beads alone) whereas no impact on T24A was observed (Fig. 3B). To ascertain the impact of CK2α phosphorylation on cortactin-mediated Arp2/3 activation, actin assembly assays were conducted with CK2α-phosphorylated cortactin and N-WASp VCA domain. As previously determined, CK2α phosphorylation of N-WASp VCA results in a modest reduction of Arp2/3 NPF activity (black vs. grey, Fig. 3C, (25)). Similarly, WT cortactin incubated with increasing amounts of CK2α prior to inclusion in polymerization assays resulted in a dose dependent suppression of actin assembly, suggesting that CK2α phosphorylation impairs the ability of cortactin to activate Arp2/3 complex (Fig. 3C). Although Arp2/3 can be activated by direct phosphorylation from multiple kinases (39–41), CK2α had no direct effect on Arp2/3 activation (orange vs. pale green, Fig. 3C), suggesting that the inhibitory effect on Arp2/3 activity is due to phosphorylated cortactin in these assays. To determine if the CK2α-targeted T24 residue is responsible for the observed inhibitory effect on Arp2/3 activity, polymerization assays were conducted with WT and T24A cortactin proteins following incubation with CK2α. While CK2α inhibited the ability of WT cortactin to activate Arp2/3 complex (blue vs. red, Fig. 3D), preincubation of CK2α with T24A cortactin exhibited no additional inhibitory effect on Arp2/3 nucleation activity (green vs. purple, Fig. 3D). Collectively these data indicate that cortactin phosphorylation at T24 by CK2α reduces the ability of cortactin to bind and activate Arp2/3 complex-mediated branched actin network formation.

CK2α is required for optimal HNSCC invadopodia function

To determine if CK2α impacts invadopodia function, CK2α expression was stably knocked down in OSC19 and UMSCC1 cells using anti-CK2α shRNAs targeting two different regions in the CK2α transcript. Both shRNAs reduced CK2α expression to non-detectable levels in each cell line (Fig. 4A). Neither line expressed the alternative CK2α' isoform in control or CK2α knockdown cells (data not shown). CK2α knockdown in OSC19 cells reduced the level of active invadopodia by 71-88% and ECM degradation by 63-73%, whereas knockdown in UMSCC1 cells reduced active invadopodia formation by 68-92% and ECM degradation by 36-60% (Fig. 4B-D). While these data indicate that CK2α is a key mediator of invadopodia maturation and function, neither invadopodia formation nor matrix degradation was entirely abolished. This would indicate that alternative signaling pathways impinging on cortactin and other invadopodia proteins remain active in the absence of CK2α expression.

The CK2α inhibitor Silmitasertib suppresses invadopodia function in HNSCC cells

Silmitasertib (CX-4945) is an orally bioavailable small molecule ATP-competitive inhibitor that targets CK2α kinase activity and is currently undergoing clinical trials in multiple cancer types (20) (NCT01199718, NCT02128282, NCT00891280). To determine the impact of Silmitasertib on HNSCC tumor cell-mediated invadopodia formation and ECM degradation, established HNSCC cell lines were treated with increasing Silmitasertib concentrations and evaluated for effects on invadopodia activity and ECM degradation.

Dose-dependent decreases in ECM degradation were observed at concentrations above 0.5 μM in all evaluated HNSCC lines (Fig. 5A & B). The greatest impairment of gelatin degradation was seen at 10 μM (Fig. 5A & B), comparable to effective CK2 specific growth-inhibitory doses in several cancer cell lines (20,42). At this concentration, active invadopodia formation was significantly diminished in OSC19 and UMSCC1 cells, whereas MDA1586 cells displayed non-significant decreases (Fig. 5C). To determine if the invadopodia inhibitory effect of Silmitasertib was directly due to altering CK2α-mediated cortactin T24 phosphorylation, antibodies against phosphorylated cortactin T24 peptides (pT24) were designed and purified. Attempts by two different commercial vendors failed to generate a pT24-specific antibody (not shown). Therefore, we evaluated the phosphorylation status of S473 (pS473) in AKT following Silmitasertib treatment as a surrogate marker for drug efficacy, as this site is known to be phosphorylated by CK2α (20). MDA1586 cells treated with 1 or 10 μM Silmitasertib had decreased pS473 AKT after 24 hours, the same timeframe used in ECM degradation assays (Supplementary Fig. S3). OSC19 and UMSCC1 cells had decreased pS473 AKT after treatment with 10 μM Silmitasertib for 12 hours, the time used for matrix degradation assays in these lines (Supplementary Fig. S3).

The fact that CK2α phosphorylates multiple targets aside from cortactin (20) raises the possibility that the inhibitory effect of Silmitasertib may be due to impairing phosphorylation of additional proteins involved in invadopodia function. To determine the extent of cortactin-specific CK2α phosphorylation in invadopodia-mediated ECM degradation, UMSCC1 cells expressing FLAG-WT, -T24A, and -T24D cortactin were treated with 1 μM Silmitasertib and evaluated for additional suppressive effects on matrix degradation (Fig. 5D & E). Silmitasertib diminished ECM degradation in cells expressing FLAG-WT cortactin by 51%, similar to the reduction observed in non-transfected cells (Fig 5D vs. B). Neither FLAG-T24A nor FLAG-T24D expressing cells treated with Silmitasertib demonstrated reductions in ECM degradation levels from baseline vehicle-treated controls (Fig. 5D & E). While these results do not entirely negate alternative CK2-dependent signaling pathways in invadopodia regulation, it does suggest that cortactin T24 is the primary CK2α target in governing HNSCC invadopodia function.

To evaluate the anti-invadopodia effect of Silmitasertib in more translationally-relevant models, patient-derived xenografts (PDXs) were derived from a well- and a moderately-differentiated HNSCC surgical sample. PDX tumors maintained original patient tumor architecture, displaying collective invasion and keratin pearls characteristic of differentiated HNSCC (Fig. 6A). Primary cell lines derived from these PDX tumors form invadopodia and spontaneously degrade gelatin within 24 hours (Fig. 6B). Both lines exhibit tight colony morphology under cell culture conditions consistent with HNSCC lines derived from epithelial HNSCC (Fig. 6B, (32,43)). Treatment of WVUSCC-AR2 and WVUSCC-AR5 with Silmitasertib yielded similar results to those observed in established lines, with gelatin degradation impaired 38-62% in WVUSCC-AR2 cells and 56-66% in WVUSCC-AR5 cells at and above 0.5 μM (Fig. 6C & D). Similarly, 10 μM Silmitasertib treatment suppressed active invadopodia by 76% in WVUSCC-AR2 and 91% in WVUSCC-AR5 (Fig. 6E). Collectively these data indicate that CK2α kinase activity is essential for maximal ECM degradation ability in HNSCC.

Silmitasertib inhibits HNSCC invasion

To determine if Silmitasertib impacts HNSCC invasion, we initially utilized a 3D *in vitro* assay designed to model collective invasion typically observed in differentiated HNSCC. Tumor spheroids generated from OSC19, UMSCC1 and WVUSCC-AR5 PDX lines were embedded between layers of collagen I. WVUSCC-AR2 cells failed to form spheroids and could not be used in this assay. Spheroids were treated with 10 μM Silmitasertib or vehicle (DMSO) for 48 h (Fig. 7A & B). Silmitasertib significantly reduced 3D collective invasion in all assayed lines (Fig. 7B). We next evaluated the ability of Silmitasertib to control invasion in the tongues of mice harboring orthotopic tumors. Luciferase-expressing UMSCC1 cells injected into the tongues of NSG mice formed detectable tumors within one week (Fig. 7C). Mice were divided into two groups containing similar tumor size as determined by *in vivo* bioluminescence, with one group treated with vehicle and one with Silmitasertib. Mice dosed twice daily for three weeks displayed a non-significant reduction in tumor growth compared to controls, similar to previous single agent xenograft studies (Fig. 7C, (20)). To negate potential bias due to unequal tumor size, four equivalent tumors from each group were selected for further assessment. In-depth evaluation of tumor margins from tongues excised after four weeks revealed alterations in invasive characteristics of Silmitasertib-treated mice (Fig. 7D-I). Tumors in drug-treated mice had a less ragged appearance at the invasive front, exhibiting shorter and smaller collective cell protrusions into the tongue stroma compared to control mice (Fig. 7D-G). In addition, tongues from Silmitasertib-treated mice had reduced perineural invasion of nerves adjacent to the invasive front (Fig. 7H & I). No difference was seen in the size or invasive distance of detached collective groups within the invasive front (Supplementary Fig. S4). Collectively these data support a role for CK2α signaling in driving several pro-invasive behaviors associated with poor patient outcome in HNSCC (2,44).

Discussion

Proteolysis of restrictive tissue barriers is essential to all steps in the metastatic cascade and increasing evidence indicates that the proteolytic activity of invadopodia is required for invasive breaching of ECM barriers (1). Signals that govern invadopodia are dynamic and highly regulated, requiring coordinated activity of several oncogenic pathways in parallel to achieve maximal efficiency (1). Active assembly and turnover of cellular F-actin networks is required for initiating invadopodia formation and subsequent maturation, involving recruitment and activation of membrane-bound and secreted MMPs to mediate ECM proteolysis (1). Breakdown of existing F-actin networks, in conjunction with Arp2/3 activation in invadopodia, is responsible for actin network turnover necessary for productive branched F-actin formation that drives membrane protrusion. Early recruitment of cortactin is necessary for invadopodia initiation, where phosphorylation of C-terminal tyrosines 421, 470, and 486, along with serines 405 and 418, occurs downstream of growth factor and integrin signaling (45). These phosphorylation events create binding sites for scaffolding platforms that recruit N-WASp and WAVE2, ensuring that activation of Arp2/3 is maintained throughout the invadopodia cycle (6). Cortactin also recruits the F-actin severing protein cofilin to invadopodia, providing the necessary machinery for cyclic actin network breakdown and regrowth during invadopod extension (16). In addition to these important C-

terminal functions, the ability of the NTA region to directly bind Arp2/3 is also essential for invadopodia formation and ECM degradation, presumably through direct Arp2/3 activation and prolonged stabilization of Arp2/3-F-actin networks (10,16).

Regarding the ability of the cortactin NTA to bind Arp2/3, this study reveals two distinct findings. First, that T24 is required for Arp2/3 binding, since mutation of this residue ablates (A) or reduces (D) the association of cortactin with Arp2/3 in co-immunoprecipitation assays. T24 is two residues C-terminal to the well-defined DDW Arp2/3 interaction motif that is conserved in other Arp2/3 NPFs (6). This places T24 in close proximity to contribute to Arp2/3 binding. While the crystal structure of the cortactin NTA bound to Arp2/3 complex has not been reported, previous chemical crosslinking and three-dimensional reconstruction studies indicate that the NTA region primarily binds the Arp3 subunit in the complex, with the most N-terminal residues spanning the Arp2-Arp3 interface to contact the Arp2 subunit (Visual Overview, (9,34)). Thus, T24 may contribute essential hydrogen bonding with recipient polar residues near the basic side chains on Arp3 involved in electrostatic binding to the acidic NTA residues. This concept is supported by the requirement of W22 in the DDW motif for Arp2/3 binding, along with the lack of an equivalent threonine in the VCA region of WASp proteins (16,34,35). While T24A cortactin appears incapable of binding Arp2/3, it can activate Arp2/3 actin nucleation in conditions where ΔDDW cortactin remains inactive (Fig. 1D). This may be due to T24 having a lower affinity for Arp3 than the DDW region and/or the high cortactin molar levels required to stimulate NPF activity *in vitro*. Nonetheless, the requirement for cortactin T24 in invadopodia-mediated ECM degradation supports an essential biological role for this residue in a non-phosphorylated context.

Secondly, our study shows that T24 phosphorylation serves to negatively regulate cortactin binding to and activation of Arp2/3 complex (Fig. 3B-D). Addition of the phosphate group to T24 likely imparts a steric and electrostatic disruption, preventing the DDW and other interacting residues in the NTA from initiating and/or maintaining binding to Arp3. Steric interference may be the predominant mechanism, since T24D cortactin can bind Arp2/3 at reduced levels (Fig. 1B), indicating that negative charge alone is insufficient to completely prevent Arp2/3 association. Phosphorylation of T24 therefore serves to block the ability of cortactin to bind Arp2/3, similar to the regulation of the Arp2/3-F-actin regulatory proteins coronin 1B and cofilin (46,47). While we did not determine if phosphorylation of T24 serves to release cortactin from existing Arp2/3-F-actin branchpoints, phosphorylation of Arp2/3-bound cortactin T24 may be an additional mechanism to dissociate cortactin from these regions. Such a mechanism could function in facilitating breakdown and recycling of invadopodia Arp2/3-F-actin networks.

The ability of CK2α to phosphorylate cortactin T24 supports a wider role for this kinase in actin regulation. Previous work identified T23 as a putative but unconfirmed CK2α phosphorylation site in the NTA region of myeloid-cell specific cortactin homolog HS1 (21). In addition, CK2α phosphorylates two adjacent sites in the A domain of WASp family proteins (22–25). These studies report conflicting results on Arp2/3 activity, with phosphorylation of WASp enhancing and in N-WASp and WAVE2 inhibiting VCA-stimulated Arp2/3-mediated actin polymerization. Our results with CK2α-phosphorylated

N-WASp VCA domain also shows an inhibitory effect on Arp2/3 activation (Fig. 3C), suggesting that CK2α effects may be differential to specific WASp family proteins.

Cortactin T24A and T24D expression in KD HNSCC lines impairs active invadopodia formation and subsequent ECM degradation (Fig. 2A-C, Supplementary Fig. 1A & C), supporting *in vitro* evidence that T24 phosphorylation prevents Arp2/3 binding and activation necessary for invadopodia activity. The importance of CK2α-mediated cortactin T24 phosphorylation is further supported by the inability of Silmitasertib to further suppress ECM degradation in cortactin T24A or T24D expressing cells (Fig. 5D & E). CK2α-specific knockdown or pharmacologic inhibition in cells would therefore be expected to reduce phosphorylation of cortactin and WASp family proteins, resulting in net increased Arp2/3 activity as observed from *in vitro* studies. The fact that CK2α knockdown or kinase blockade also impairs invadopodia formation and function is paradoxical, but can be explained by cyclic CK2α phosphorylation and dephosphorylation to regulate cortactin binding to and activation of Arp2/3 in invadopodia during maturation and elongation. Dephosphorylation of cortactin T24 and WASp NPFs by unknown phosphatases would enable these NPFs to promote Arp2/3 activation, actin polymerization, and invadopodia activity. Following network breakdown during actin turnover, CK2α phosphorylation would return NPFs to the inactive state to await the next cycle of actin assembly. While similar cyclic regulation of Src and cofilin has been shown to be essential for invadopodia function and provides support for this model (38,46), confirmation of T24 phosphorylation within invadopodia leading to altered actin dynamics along with identification of the T24 phosphatase are necessary to fully confirm this proposed mechanism.

Locoregional control of HNSCC dissemination is problematic, where perineural invasion and invasive metastatic spread to cervical lymph nodes accelerates patient decline (44,48,49). Cortactin and CK2α expression are elevated in HNSCC and individually correspond with poorer patient outcomes (7,20). CK2 knockdown and Silmitasertib treatment in HNSCC cells has anti-proliferative and anti-metastatic properties *in vitro* and in mice, providing support for the utility of Silmitasertib in HNSCC (20). The anti-invasive effect of Silmitasertib shown here is likely due in part to disruption of the invadopodia actin assembly through combined inhibition of multiple Arp2/3 NPFs. We note that T24 cortactin mutants, CK2α knockdown, and Silmitasertib treatment in HNSCC cells does not completely abolish invadopodia formation, degradation activity or invasion. Activation of invadopodial Arp2/3 NPFs through alternative scaffolding or lipid-based signaling pathways that can bypass CK2 inhibition can account for this residual activity (1). However, our results indicate that CK2α inhibition by a single agent does significantly impair collective HNSCC invasion. Given the current paucity of treatment options for invasive HNSCC, combining Silmitasertib with additional drugs known to impair invadopodia function by blocking additional invadopodia and motility pathways (8) has the potential to provide novel treatment options for controlling invasive spread of late-stage HNSCC harboring elevated cortactin and/or CK2 expression.

Supplementary Material

Refer to Web version on PubMed Central for supplementary material.

Acknowledgments

We thank Jianjiong Gao (University of Missouri) for sequence prediction analysis. The assistance of the West Virginia University Microscope Imaging Facility, Animal Models and Imaging Facility, and Biochemistry Protein Core are gratefully acknowledged.

This work was supported by pilot grants from NIH U54GM104942, P20RR016440 and P20GM103434 (S. Markwell, A. Ammer, J. Allen, B. Papenberg, R. Hames, S. Weed). Additional support was provided by the West Virginia University Department of Neurobiology and Anatomy (S. Markwell, S. Weed), Department of Biochemistry (S. Markwell, S. Weed), Department of Otolaryngology, Head and Neck Surgery (E. Interval, J. Castaño), and the Dorothy D. Radford Endowed Fund of the West Virginia University Cancer Institute (S. Weed). Instrumentation support was provided by NIH grants U54GM104942, P20RR016440, P30RR032138/GM103488, P20GM103434, and P20RR016477.

References

1. Eddy RJ, Weidmann MD, Sharma VP, Condeelis JS. Tumor Cell Invadopodia: Invasive Protrusions that Orchestrate Metastasis. Trends Cell Biol. Elsevier Ltd; 2017;27:595–607.
2. Markwell S, Weed S. Tumor and Stromal-Based Contributions to Head and Neck Squamous Cell Carcinoma Invasion. Cancers (Basel). 2015;7:382–406. [PubMed: 25734659]
3. Bowden ET, Barth M, Thomas D, Glazer RI, Mueller SC. An invasion-related complex of cortactin, paxillin and PKCmu associates with invadopodia at sites of extracellular matrix degradation. Oncogene. 1999;18:4440–9. [PubMed: 10442635]
4. Branch KM, Hoshino D, Weaver AM. Adhesion rings surround invadopodia and promote maturation. Biol Open. 2012;1:711–22. [PubMed: 23213464]
5. Schnoor M, Stradal TE, Rottner K. Cortactin: Cell Functions of A Multifaceted Actin-Binding Protein. Trends Cell Biol. 2018;28:79–98. [PubMed: 29162307]
6. Yin M, Ma W, An L. Cortactin in cancer cell migration and invasion. Oncotarget. Impact Journals, LLC; 2017;8:88232–43.
7. MacGrath SM, Koleske AJ. Cortactin in cell migration and cancer at a glance. J Cell Sci. Company of Biologists; 2012;125:1621–6.
8. Meirson T, Gil-Henn H. Targeting invadopodia for blocking breast cancer metastasis. Drug Resist Updat. 2018;39:1–17. [PubMed: 30075834]
9. Xu X-P, Rouiller I, Slaughter BD, Egile C, Kim E, Unruh JR, et al. Three-dimensional reconstructions of Arp2/3 complex with bound nucleation promoting factors. EMBO J. Nature Publishing Group; 2012;31:236–47.
10. Weaver AM, Karginov AV., Kinley AW, Weed SA, Li Y, Parsons JT, et al. Cortactin promotes and stabilizes Arp2/3-induced actin filament network formation. Curr Biol. 2001;11:370–4. [PubMed: 11267876]
11. Helgeson LA, Prendergast JG, Wagner AR, Rodnick-Smith M, Nolen BJ. Interactions with Actin Monomers, Actin Filaments and Arp2/3 Complex Define the Roles of WASP Family Proteins and Cortactin in Coordinately Regulating Branched Actin Networks. J Biol Chem. 2014;289:1–26. [PubMed: 24257748]
12. Weed SA, Karginov AV., Schafer DA, Weaver AM, Kinley AW, Cooper JA, et al. Cortactin localization to sites of actin assembly in lamellipodia requires interactions with F-actin and the Arp2/3 complex. J Cell Biol. 2000;151:29–40. [PubMed: 11018051]
13. Weaver AM, Young ME, Lee W-L, Cooper JA. Integration of signals to the Arp2/3 complex. Curr Opin Cell Biol. 2003;15:23–30. [PubMed: 12517700]
14. Blanchoin L, Amann KJ, Higgs HN, Marchand J, Kaiser DA, Pollard TD. Direct observation of dendritic actin filament networks nucleated by Arp2/3 complex and WASP / Scar proteins. Nature. 2000;404:1007–11. [PubMed: 10801131]
15. Martinez-quiles N, Ho HH, Kirschner MW, Ramesh N, Geha RS. Erk / Src Phosphorylation of Cortactin Acts as a Switch On-Switch Off Mechanism That Controls Its Ability To Activate N-WASP. Mol Cell Biol. 2004;24:5269–80. [PubMed: 15169891]

16. Oser M, Yamaguchi H, Mader CC, Bravo-Cordero JJ, Arias M, Chen X, et al. Cortactin regulates cofilin and N-WASp activities to control the stages of invadopodium assembly and maturation. J Cell Biol. 2009;186:571–87. [PubMed: 19704022]
17. Mader CC, Oser M, Magalhaes MAO, Bravo-Cordero JJ, Condeelis J, Koleske AJ, et al. An EGFR-Src-Arg-Cortactin pathway mediates functional maturation of invadopodia and breast cancer cell invasion. Cancer Res. 2011;71:1730–41. [PubMed: 21257711]
18. Ayala I, Baldassarre M, Giacchetti G, Caldieri G, Tetè S, Luini A, et al. Multiple regulatory inputs converge on cortactin to control invadopodia biogenesis and extracellular matrix degradation. J Cell Sci. 2008;121:369–78. [PubMed: 18198194]
19. Martin KH, Jeffery ED, Grigera PR, Shabanowitz J, Hunt DF, Parsons JT. Cortactin phosphorylation sites mapped by mass spectrometry. J Cell Sci. 2006;119:2851–3. [PubMed: 16825425]
20. Chua MMJ, Ortega CE, Sheikh A, Lee M, Abdul-Rassoul H, Hartshorn KL, et al. CK2 in Cancer: Cellular and Biochemical Mechanisms and Potential Therapeutic Target Pharmaceuticals (Basel). Multidisciplinary Digital Publishing Institute (MDPI); 2017;10.
21. Ruzzene M, Brunati AM, Sarno S, Marin O, Donella-Deana A, Pinna LA. Ser/Thr phosphorylation of hematopoietic specific protein 1 (HS1): implication of protein kinase CK2. Eur J Biochem. 2000;267:3065–72. [PubMed: 10806407]
22. Mendoza MC. Phosphoregulation of the WAVE regulatory complex and signal integration. Semin Cell Dev Biol. Elsevier Ltd; 2013;24:272–9.
23. Pocha SM, Cory GO. WAVE2 is regulated by multiple phosphorylation events within its VCA domain. Cell Motil Cytoskeleton. 2009;66:36–47. [PubMed: 19012317]
24. Cory GOC, Cramer R, Blanchoin L, Ridley AJ. Phosphorylation of the WASP-VCA domain increases its affinity for the Arp2/3 complex and enhances actin polymerization by WASP. Mol Cell. 2003;11:1229–39. [PubMed: 12769847]
25. Galovic M, Xu D, Areces LB, van der Kammen R, Innocenti M. Interplay between N-WASP and CK2 optimizes clathrin-mediated endocytosis of EGFR. J Cell Sci. 2011;124:2001–12. [PubMed: 21610097]
26. Hayes KE, Walk EL, Ammer AG, Kelley LC, Martin KH, Weed SA. Ableson Kinases Negatively Regulate Invadopodia Function and Invasion in Head and Neck Squamous Cell Carcinoma by Inhibiting an HB-EGF Autocrine Loop. Oncogene. 2013;32:4766–77. [PubMed: 23146907]
27. Ammer AG, Kelley LC, Hayes KE, Evans J V, Lopez-skinner A, Martin KH, et al. Saracatinib impairs head and neck squamous cell carcinoma invasion by disruption invadopodia function. J Cancer Sci Ther. 2009;1:52–61. [PubMed: 20505783]
28. Head JA, Jiang D, Li M, Zorn LJ, Schaefer EM, Parsons JT, et al. Cortactin Tyrosine Phosphorylation Requires Rac1 Activity and Association with the Cortical Actin Cytoskeleton. Mol Biol Cell. 2003;14:3216–29. [PubMed: 12925758]
29. Martin KH, Hayes KE, Walk EL, Ammer AG, Markwell SM, Weed SA. Quantitative Measurement of Invadopodia-mediated Extracellular Matrix Proteolysis in Single and Multicellular Contexts. J Vis Exp. 2012;e4119. [PubMed: 22952016]
30. Kelley LC, Weed SA. Cortactin Is a Substrate of Activated Cdc42-Associated Kinase 1 (ACK1) during Ligand-induced Epidermal Growth Factor Receptor Downregulation. PLoS One. 2012;7:e44363. [PubMed: 22952966]
31. Mooren OL, Kotova TI, Moore AJ, Schafer DA. Dynamin2 GTPase and cortactin remodel actin filaments. J Biol Chem. 2009;284:23995–4005. [PubMed: 19605363]
32. Basu D, Nguyen T-TK, Montone KT, Zhang G, Wang L-P, Diehl JA, et al. Evidence for mesenchymal-like sub-populations within squamous cell carcinomas possessing chemoresistance and phenotypic plasticity. Oncogene. 2010;29:4170–82. [PubMed: 20498638]
33. Gatesman Ammer A, Hayes KE, Martin KH, Zhang L, Spirou GA, Weed SA. Multi-photon Imaging of Tumor Cell Invasion in an Orthotopic Mouse Model of Oral Squamous Cell Carcinoma. J Vis Exp. 2011;1–7.
34. Weaver AM, Heuser JE, Karginov A V., Lee W, Parsons JT, Cooper JA. Interaction of cortactin and N-WASp with Arp2/3 complex. Curr Biol. 2002;12:1270–8. [PubMed: 12176354]

35. Uruno T, Liu J, Zhang P, Fan Y, Egile C, Li R, et al. Activation of Arp2/3 complex-mediated actin polymerization by cortactin. Nat Cell Biol. 2001;3:259–66. [PubMed: 11231575]
36. Clark ES, Whigham AS, Yarbrough WG, Weaver AM. Cortactin is an essential regulator of matrix metalloproteinase secretion and extracellular matrix degradation in invadopodia. Cancer Res. 2007;67:4227–35. [PubMed: 17483334]
37. Siton O, Ideses Y, Albeck S, Unger T, Bershadsky AD, Gov NS, et al. Cortactin releases the brakes in actin- based motility by enhancing WASP-VCA detachment from Arp2/3 branches. Curr Biol. Elsevier Ltd; 2011;21:2092–7.
38. Kelley LC, Ammer AG, Hayes KE, Martin KH, Machida K, Jia L, et al. Oncogenic Src requires a wild-type counterpart to regulate invadopodia maturation. J Cell Sci. 2010;123:3923–32. [PubMed: 20980387]
39. Vadlamudi RK, Li F, Barnes CJ, Bagheri-Yarmand R, Kumar R. p41-Arc subunit of human Arp2/3 complex is a p21-activated kinase-1-interacting substrate. EMBO Rep. 2004;5:154–60. [PubMed: 14749719]
40. Kazazian K, Go C, Wu H, Brashavitskaya O, Xu R, Dennis JW, et al. Plk4 Promotes Cancer Invasion and Metastasis through Arp2/3 Complex Regulation of the Actin Cytoskeleton. Cancer Res. 2017;77:434–47. [PubMed: 27872092]
41. LeClaire LL, Rana M, Baumgartner M, Barber DL. The Nck-interacting kinase NIK increases Arp2/3 complex activity by phosphorylating the Arp2 subunit J Cell Biol. Rockefeller University Press; 2015;208:161–70. [PubMed: 25601402]
42. Siddiqui-Jain A, Drygin D, Streiner N, Chua P, Pierre F, O'Brien SE, et al. CX-4945, an orally bioavailable selective inhibitor of protein kinase CK2, inhibits prosurvival and angiogenic signaling and exhibits antitumor efficacy. Cancer Res. American Association for Cancer Research; 2010;70:10288–98.
43. Zhao M, Sano D, Pickering CR, Jasser SA, Henderson YC, Clayman GL, et al. Assembly and initial characterization of a panel of 85 genomically validated cell lines from diverse head and neck tumor sites. Clin Cancer Res. 2011;17:7248–64. [PubMed: 21868764]
44. Kurtz KA, Hoffman HT, Bridget Zimmerman M, Robinson RA, Carver LA. Perineural and Vascular Invasion in Oral Cavity Squamous Carcinoma Increased Incidence on Re-review of Slides and by Using Immunohistochemical Enhancement. Arch Pathol Lab Med. 2005.
45. Kelley LC, Hayes KE, Ammer AG, Martin KH, Weed SA. Cortactin phosphorylated by ERK1/2 localizes to sites of dynamic actin regulation and is required for carcinoma lamellipodia persistence. PLoS One. 2010;5:e13847. [PubMed: 21079800]
46. Oser M, Condeelis J. The cofilin activity cycle in lamellipodia and invadopodia. J Cell Biochem. 2009;108:1252–62. [PubMed: 19862699]
47. Cai L, Holoweckyj N, Schaller MD, Bear JE. Phosphorylation of coronin 1B by protein kinase C regulates interaction with Arp2/3 and cell motility. J Biol Chem. 2005;280:31913–23. [PubMed: 16027158]
48. Xing Y, Zhang J, Lin H, Gold KA, Sturgis EM, Garden AS, et al. Relation between the level of lymph node metastasis and survival in locally advanced head and neck squamous cell carcinoma. Cancer. 2016;122:534–45. [PubMed: 26554754]
49. Fagan JJ, Collins B, Barnes L, D'Amico F, Myers EN, Johnson JT. Perineural Invasion in Squamous Cell Carcinoma of the Head and Neck Arch Otolaryngol Neck Surg. American Medical Association; 1998;124:637.

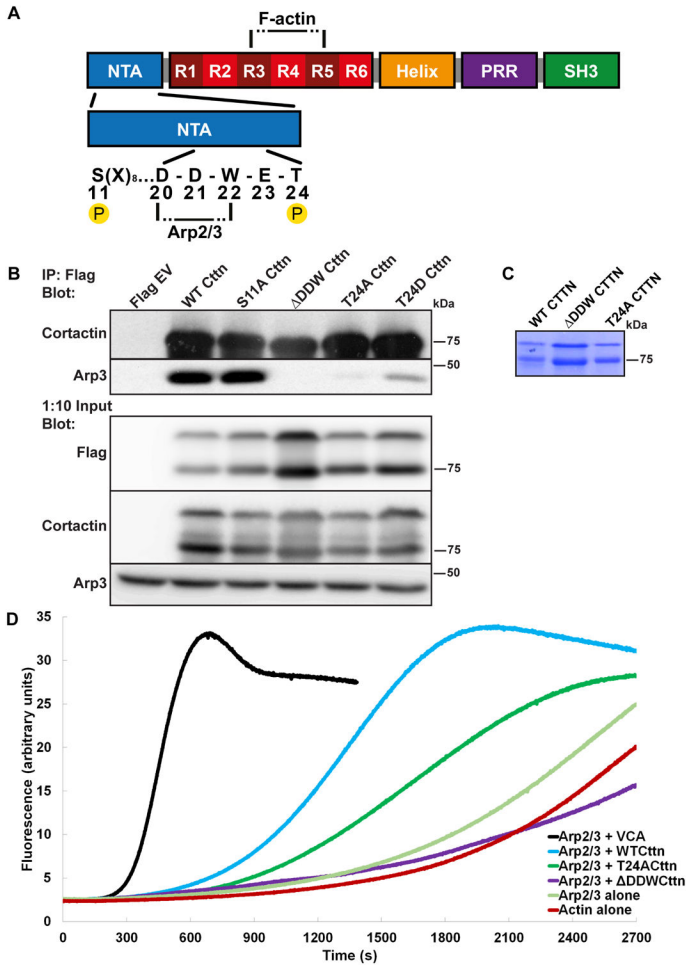

Figure 1. Cortactin T24 is required for binding and activation of Arp2/3 complex.

A. Diagram representing cortactin functional domains. NTA, N-terminal acidic domain; R1-R6, repeats regions with F-actin binding site indicated; Helix, alpha helical domain, PRR, proline rich region; SH3, Src homology 3 domain. NTA domain with position of S11 and T24 in context of the DDW region is shown. B. Immunoprecipitation analysis of Arp2/3 binding to cortactin NTA mutants. HEK293T/17 cells transfected with FLAG-empty vector (EV), FLAG-wild-type cortactin (WT) or the indicated FLAG-cortactin mutants. Immune complexes were Western blotted with antibodies against cortactin (top) and Arp3 (bottom). 1:10 diluted total cell lysates were Western blotted as indicated. C. Coomassie blue staining of the indicated purified recombinant human cortactin proteins. D. Effect of cortactin T24A on Arp2/3 complex activation. Fluorometric evaluation of actin polymerization over time with the indicated cortactin mutants incubated with Arp2/3 complex and pyrene-labeled actin. Polymerization curves: WT cortactin (blue); T24A cortactin (dark green) and ΔDDW cortactin (purple). N-WASp VCA domain (black) was used as a positive control; negative controls include Arp2/3 complex plus actin (pale green) and actin alone (red). Polymerization curves are representative from three independent experiments.

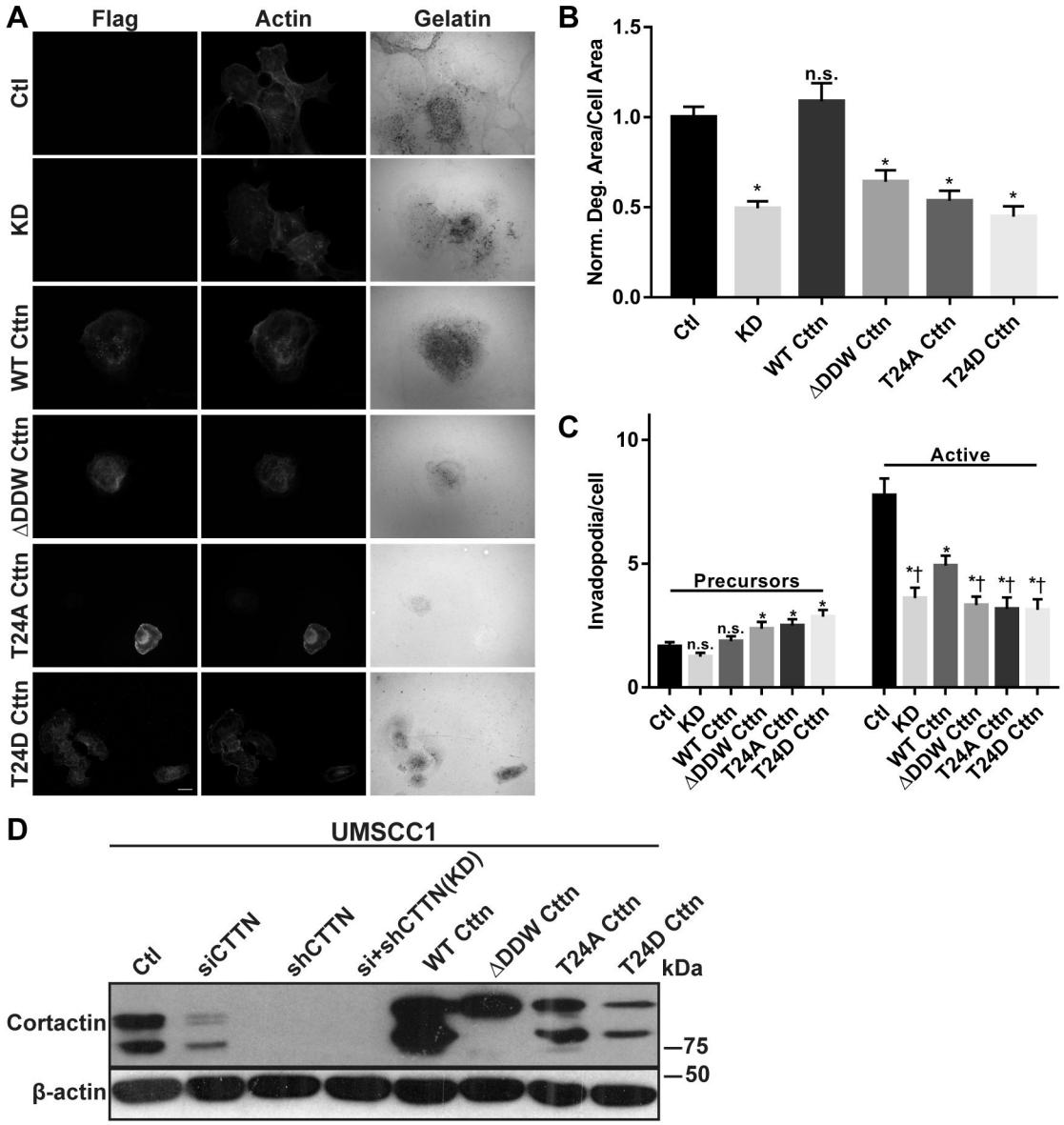

Figure 2. T24 is required for cortactin-mediated invadopodia formation and ECM degradation in HNSCC cells.

A. UMSCC1 cells with stable shRNA scramble control (Ctl) or anti-cortactin shRNA combined with siRNA knockdown (KD) were transduced with murine FLAG-WT, -ΔDDW, -T24A and -T24D cortactin lentiviruses. Cells were plated on Oregon Green (OG)-488 gelatin coated coverslips for 12 hours, fixed, and labeled with anti-FLAG and rhodamine phalloidin (Actin). Gelatin panels are pseudo-colored white; degradation is evident as black areas indicating loss of fluorescence. Scale bar represents 20 μm. **B.** Quantification of gelatin matrix degradation for control (Ctl), cortactin KD and FLAG-cortactin expressing UMSCC1 cells. **C.** Quantification of invadopodia precursors (left) and active invadopodia (right) numbers from the lines assayed in (**B**). Data represents the mean + S.E.M. of n ≥ 100 cells for each line analyzed from at least three independent experiments. All gelatin degradation conditions were normalized to Ctl UMSCC1 cells. n.s., not significant; *, P <

0.05, Welch's or Student's *t* test vs. Ctl (**B** & **C)**, †, P < 0.05, Student's *t* test vs. wild type cortactin rescue (WT) (**C**). **D.** Total cell lysates from (**A**) evaluated for endogenous and FLAG-cortactin expression by immunoblotting with antibodies against cortactin (top) and β-actin (bottom).

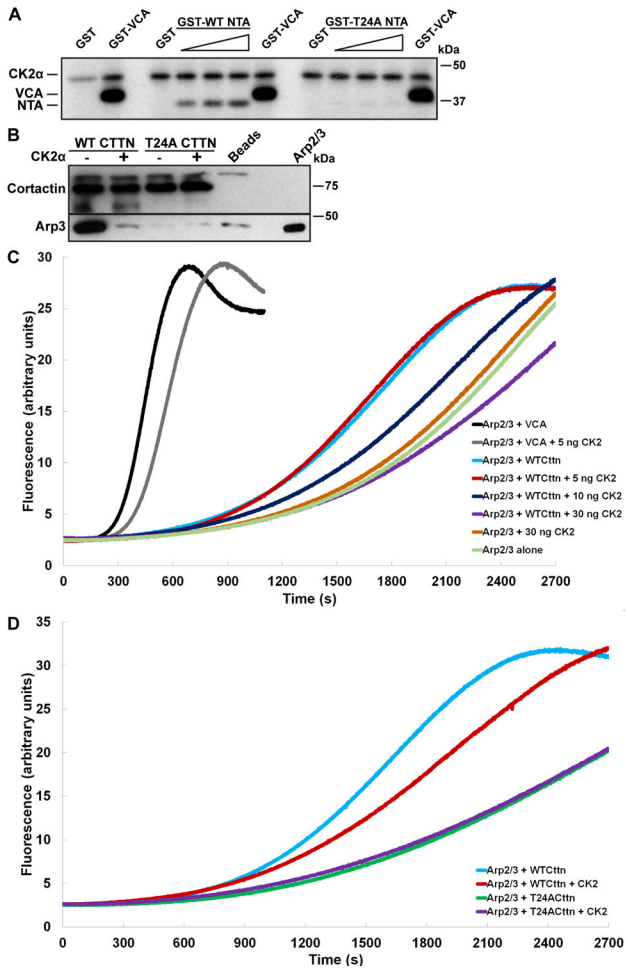

Figure 3. CK2α phosphorylation of cortactin T24 inhibits Arp2/3 complex binding and activation.

A. Cortactin T24 is a CK2α phosphorylation site. Autoradiogram of active CK2α incubated with the increasing amounts (0, 0.25, 0.5, and 1 μg) of GST-WT-NTA or GST-T24A-NTA cortactin fusion proteins. GST (1 μg) and the GST-VCA domain of N-WASp (0.25 μg) were used as respective negative and positive phosphorylation controls. Positions of autophosphorylated CK2α, GST-VCA and cortactin NTA proteins are indicated on the left; autoradiogram is representative of three independent experiments. **B.** CK2α phosphorylation at cortactin T24 ablates binding to Arp2/3 complex. Purified recombinant human WT and T24A cortactin proteins (2.5 μg) were bound with an anti-cortactin antibody to protein G beads. Immune complexes were preincubated with or without 75 ng active CK2α, washed and incubated with 50 ng purified Arp2/3 complex. Co-immunoprecipitated complexes were Western blotted for cortactin (top) and Arp3 (bottom). 4F11-bound protein G beads were used as a negative control for non-specific binding (Beads). Arp2/3 complex (5 ng) was used as positive control for Arp3 immunoblotting. Blot is representative of two independent experiments. **C.** Cortactin phosphorylation by CK2α inhibits cortactin-mediated Arp2/3 actin polymerization. WT human cortactin or GST-VCA proteins were preincubated with the indicated amounts of active CK2α and evaluated for effects on Arp2/3 activity. Polymerization curves are representative from three independent experiments. **D.**

Phosphorylation of T24 is responsible for the inhibitory effect of CK2α on cortactin-mediated Arp2/3 activation. Human WT and T24A cortactin proteins were preincubated with or without 30 ng active CK2α and evaluated for effects on Arp2/3-mediated actin assembly. Polymerization curves are representative from three independent experiments.

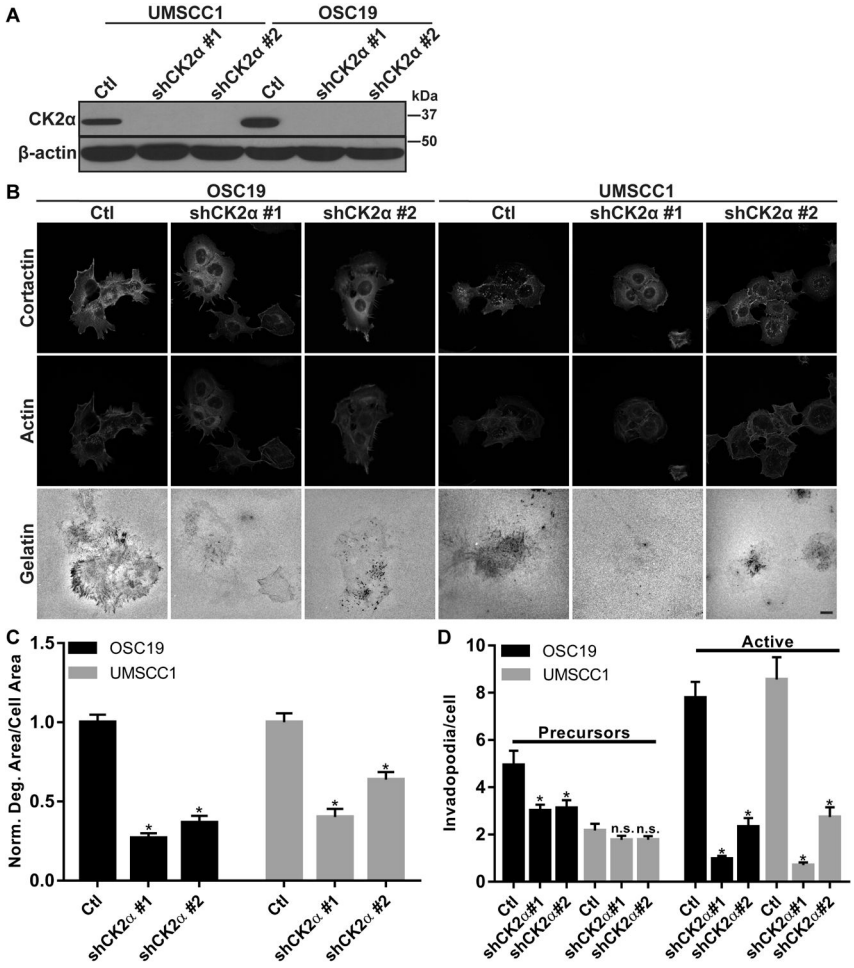

Figure 4. CK2α is required for optimal HNSCC invadopodia function.

A. Evaluation of CK2α expression in stable scramble control (Ctl) and CK2α shRNA HNSCC cells. Cells were lysed and Western blotted with antibodies against CK2α (top) and β-actin (bottom). **B.** Representative confocal images of OSC19 and UMSCC1 cells with Ctl shRNA and with each anti-CK2α shRNA (shCK2α #1 and #2). Cells were plated on OG-488 gelatin coverslips for 12 h then labeled with an anti-cortactin antibody and rhodamine phalloidin (Actin). Gelatin is pseudo-colored white. Scale bar represents 20 μm. **C.** CK2α knockdown decreases invadopodia-mediated ECM degradation. Quantification of matrix degradation area per cell area for Ctl and each anti-CK2α shRNA in the indicated cell lines. Degradation data was normalized to Ctl condition for each cell line. **D**. CK2α knockdown decreases invadopodia numbers. Amount of invadopodia precursors (left) and active invadopodia (right) per cell is shown for control and shCK2α OSC19 and UMSCC1 cells. Data in **C** and **D** represents the mean + S.E.M. of n ≥ 100 cells analyzed from at least three independent experiments. n.s., not significant; *, $P < 0.05$, Welch's *t* test vs. Ctl.

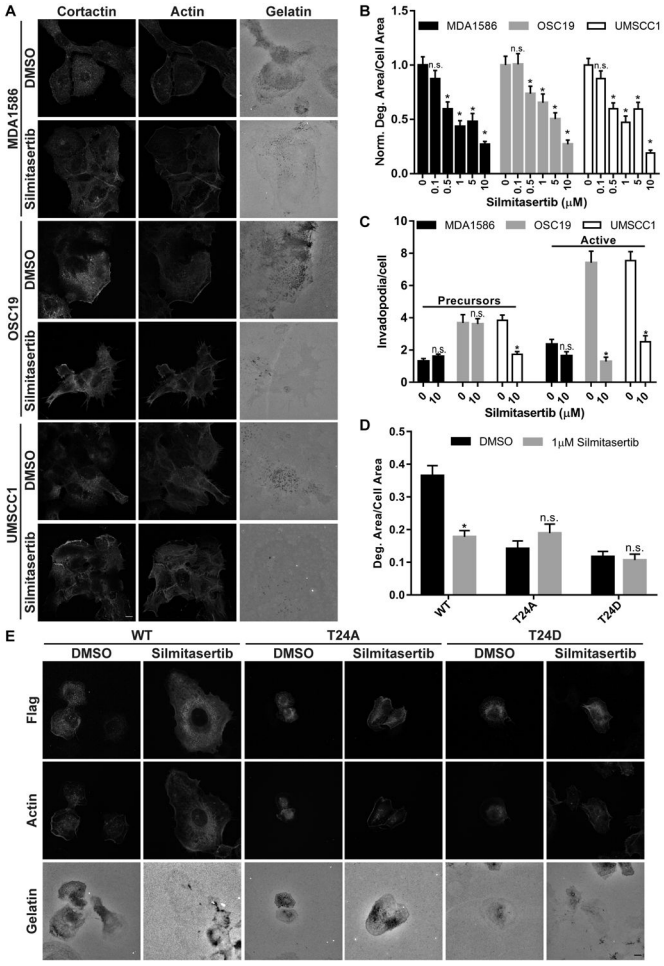

Figure 5. Silmitasertib-mediated CK2 inhibition reduces invadopodia function in established HNSCC cell lines.

A. Representative confocal images of MDA1586, OSC19, and UMSCC1 cells plated on OG-488 gelatin coverslips for 1 hour before treatment with vehicle (DMSO) or 10 μM Silmitasertib for 24 hours (MDA1586) or 12 hours (OSC19 & UMSCC1) (optimal ECM degradation times for each line). Cells were fixed and labeled with an anti-cortactin antibody and rhodamine phalloidin (Actin). Gelatin is pseudo-colored white. Scale bar represents 20 μm. **B.** CK2α inhibition decreases invadopodia-mediated ECM degradation. Quantification of gelatin matrix degradation area per cell area in HNSCC cell lines treated with the indicated Silmitasertib concentrations. **C.** CK2α inhibition decreases invadopodia numbers. Amount of invadopodia precursors (left) and active invadopodia (right) per cell is shown for Silmitasertib treated HNSCC cell lines. Degradation data was normalized to DMSO-treated (0) cells for each cell line. Data in **B** and **C** represents the mean + S.E.M. of n ≥ 100 cells analyzed from at least three independent experiments. n.s., not significant; *, $P < 0.05$, Welch's or Student's *t* test vs. DMSO for each cell line. **D.** Quantitation of gelatin matrix degradation area per cell area for UMSCC1 cells expressing FLAG-WT, -T24A or -T24D cortactin treated with DMSO or 1 μM Silmitasertib. Data represents the mean + S.E.M of n ≥ 75 cells analyzed from at least three independent experiments. n.s., not significant; *, $P < 0.05$, Welch's or Student's *t* test vs. DMSO for each condition. **E.** Representative confocal

images of UMSCC1 cells expressing FLAG-WT, -T24A, or -T24D cortactin plated on OG-488 gelatin coverslips for 1 hour before treatment with vehicle (DMSO) or 1 μM Silmitasertib for 12 hours. Cells were fixed and labeled with an anti-FLAG antibody and rhodamine phalloidin (Actin). Gelatin is pseudo-colored white. Scale bar represents 20 μm.

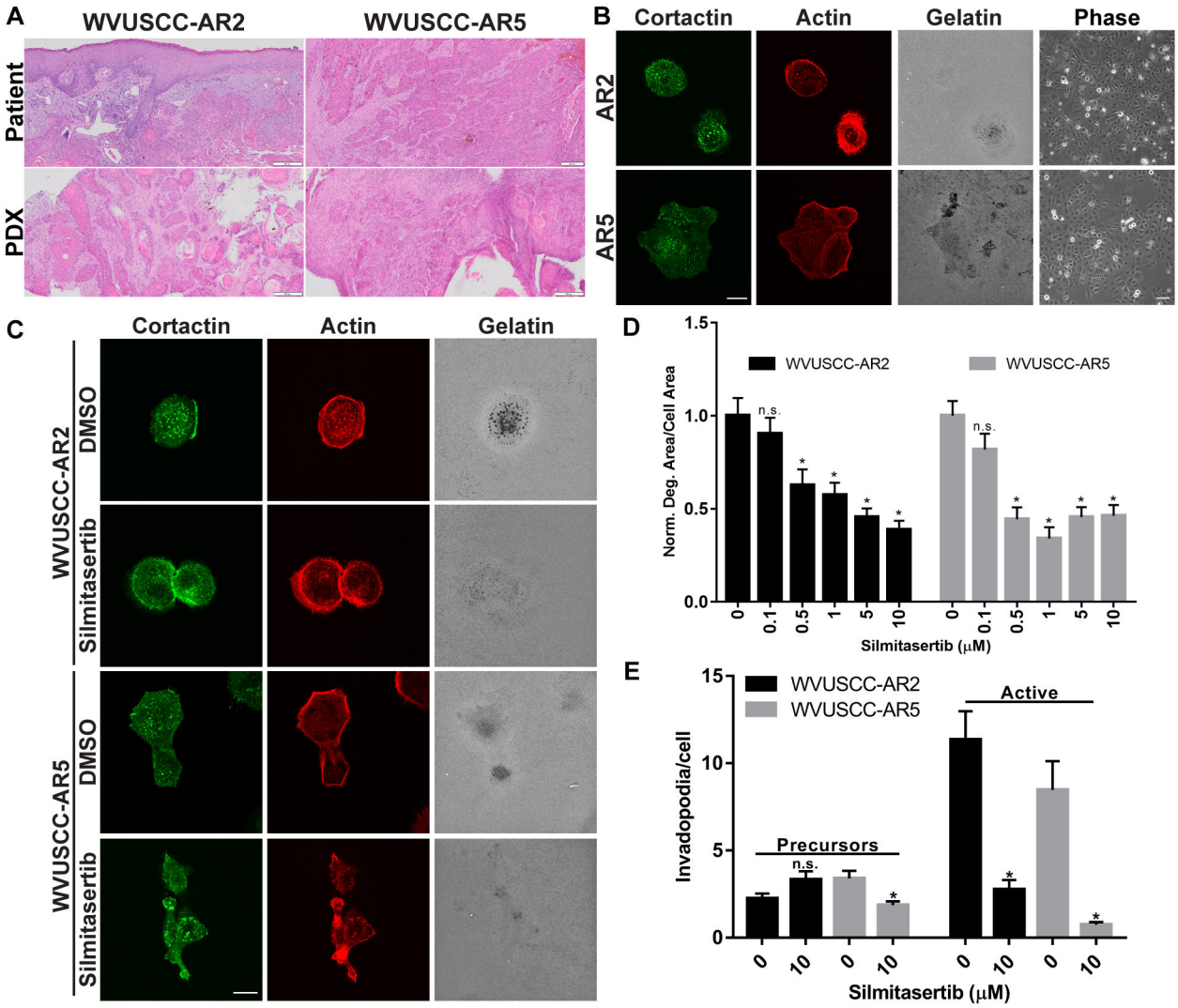

Figure 6. Silmitasertib inhibits invadopodia function in HNSCC PDX cells.

A. Establishment of HNSCC patient-derived xenograft (PDX) tumors. Hematoxylin and eosin stained patient tumor tissue and PDXs. Patient tumors were from the alveolar ridge (AR). Scale bar represents 200 μm. **B.** Invadopodia formation in HNSCC PDX cells. Representative confocal images of WVUSCC-AR2 (AR2) and WVUSCC-AR5 (AR5) PDX cell lines. Cells were plated on OG-488 gelatin coverslips for 24 hours and labeled with an anti-cortactin antibody and rhodamine phalloidin (Actin). Gelatin is pseudo-colored white. Scale bar represents 20 μm. 10X representative phase contrast images (Phase) of each line are shown on the right. Scale bar represents 100 μm. **C.** Confocal images of WVUSCC-AR2 and WVUSCC-AR5 cells plated on OG-488 gelatin coverslips, allowed to attach for 1 hour, then treated with vehicle (DMSO) or 10 μM Silmitasertib for 24 hours. Cells were labeled with an anti-cortactin antibody and rhodamine phalloidin (Actin). Gelatin is pseudo-colored white. Scale bar represents 20 μm. **D.** CK2α inhibition decreases invadopodia-mediated ECM degradation in PDX derived cell lines. Quantification of matrix degradation area per cell area for WVUSCC-AR2 and WVUSCC-AR5 PDX cell lines treated with the indicated Silmitasertib concentrations. Degradation data was normalized to DMSO-treated cells for

each cell line. **E.** CK2α inhibition decreases invadopodia numbers in PDX derived cell lines. Determination of amount of invadopodia precursors (left) and active invadopodia (right) in WVUSCC-AR2 and WVUSCC-AR5 cells. Data represents the mean + S.E.M. of n ≥ 100 cells analyzed from at least three independent experiments. *, P ˂ 0.05, Welch's *t* test vs. DMSO for each cell line.

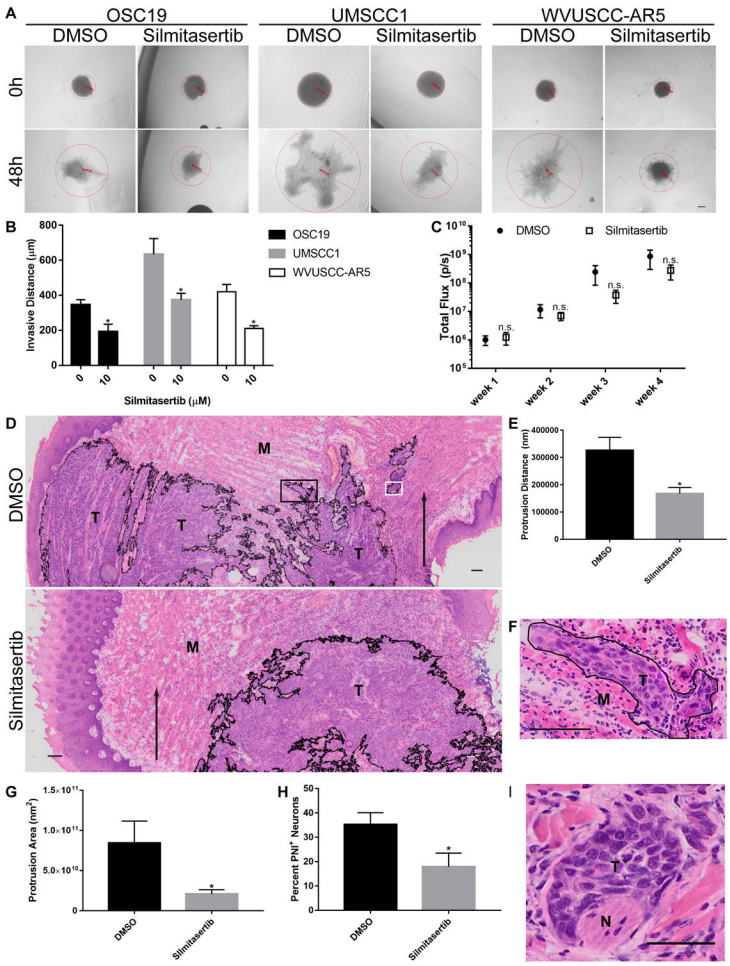

Figure 7. Silmitasertib impairs collective invasion in HNSCC.

A. Representative phase contrast microscopy images of OSC19, UMSCC1 and WVUSCC-AR5 tumor cell spheroids embedded in collagen I (0 h) then incubated in complete media containing 10 μM Silmitasertib or vehicle (DMSO) for 48 h. Red circles indicate the maximum radial distance at indicated time points. Scale bar represents 100 μm. **B.** Quantitation of maximal collective invasive distance of each cell line at 48 h with vehicle (0) or Silmitasertib (10 μM). Data represents the mean + S.E.M. of n ≥ 10 spheroids per cell line and condition analyzed from at least three independent experiments. *, $P < 0.05$, Welch's or Student's *t* test vs. DMSO. **C.** Effect of Silmitasertib on HNSCC orthotopic tumor growth. Bioluminescent monitoring of UMSCC1 cells orthotopically injected into tongues of NSG mice. Tumors were allowed to establish for one week prior to administration of Silmitasertib or equal volume vehicle (DMSO). Data represent means +/− S.E.M. from two independent experiments. DMSO, n = 9 mice; Silmitasertib, n = 7 mice. n.s., not significant; Student's *t* test vs. DMSO. **D.** Silmitasertib inhibits orthotopic HNSCC invasion. Representative hematoxylin and eosin stained invasive front of orthotopic UMSCC1 tongue tumors from mice receiving Silmitasertib or vehicle (DMSO) for three weeks. Black lines show tumor-encompassing RIO borders determined by software analysis. Black box in DMSO tumor indicates the invasive protrusion shown in **F**. White box in DMSO tumor denotes region

containing perineural invasion (PNI) shown in **I**. Black arrow indicates direction of invasion toward tongue base. M, skeletal muscle; T, tumor. Scale bar represents 100 μm. **E.** Invasive distance of tumor protrusions from mice treated with Silmitasertib or vehicle (DMSO). Data represent the mean + S.E.M. of two serial sections from N = 4 tumors; n = 34 protrusions per condition. *, $P < 0.05$, Student's *t* test vs. DMSO. **F**. Representative image of an invasive protrusion from vehicle-treated mice shown in the black box in **D**. The protrusive region was traced in black to denote the tumor protrusion from surrounding muscle-containing stroma. M, skeletal muscle; T, tumor protrusion. Scale bar represents 100 μm. **G.** Area of invasive protrusions from mice treated with Silmitasertib or vehicle (DMSO). Data represent the mean + S.E.M. of two serial sections from N = 4 tumors; n = 34 protrusions per condition. *, $P < 0.05$, Welch's *t* test vs. DMSO. **H.** Percentage of lingual nerves displaying PNI in tumors from mice treated with Silmitasertib or vehicle (DMSO). Data represent the mean + S.E.M. of two serial sections from N = 4 tumors; $n \geq 60$ nerves per condition. *, $P < 0.05$, Student's *t* test vs. DMSO. **I.** Representative image of PNI shown in the white box in the DMSO-treated mouse in **D**. N, nerve; T, tumor cells. Scale bar represents 50 μm.